SANDIA REPORT

SAND2008-6024
Unlimited Release
Printed September 2008

Size Effect in Continuum Modeling

Wei-Yang Lu, James W. Foulk III, Edwin M. Huestis, Kevin Connelly, Bo Song, and Nancy Yang

Prepared by
Sandia National Laboratories
Albuquerque, New Mexico 87185 and Livermore, California 94550

Sandia is a multiprogram laboratory operated by Sandia Corporation,
a Lockheed Martin Company, for the United States Department of Energy's
National Nuclear Security Administration under Contract DE-AC04-94AL85000.

Issued by Sandia National Laboratories, operated for the United States Department of Energy by Sandia Corporation.

Available to DOE and DOE contractors from
U.S. Department of Energy
Office of Scientific and Technical Information
P.O. Box 62
Oak Ridge, TN 37831

Telephone: (865) 576-8401
Facsimile: (865) 576-5728
E-Mail: reports@adonis.osti.gov
Online ordering: http://www.osti.gov/bridge

Available to the public from
U.S. Department of Commerce
National Technical Information Service
5285 Port Royal Rd.
Springfield, VA 22161

Telephone: (800) 553-6847
Facsimile: (703) 605-6900
E-Mail: orders@ntis.fedworld.gov
Online order: http://www.ntis.gov/help/ordermethods.asp?loc=7-4-0#online

SAND2008-6024
Unlimited Release
Printed September 2008

Size Effect in Continuum Modeling

Wei-Yang Lu, James W. Foulk III, Edwin M. Huestis, Kevin Connelly, and Bo Song
Mechanics of Materials

Nancy Y.C. Yang
Engineered Materials

Sandia National Laboratories
P.O. Box 0969
Livermore, California 94551-0969

Abstract

The mechanical properties of some materials (Cu, Ni, Ag, etc.) have been shown to develop strong dependence on the geometric dimensions, resulting in a size effect. Several theories have been proposed to model size effects, but have been based on very few experiments conducted at appropriate scales. Some experimental results implied that size effects are caused by increasing strain gradients and have been used to confirm many strain gradient theories. On the other hand, some recent experiments show that a size effect exists in the absence of strain gradients. This report describes a brief analytical and experimental study trying to clarify the material and experimental issues surrounding the most influential size-effect experiments by Fleck *et al* (1994). This effort is to understand size effects intended to further develop predictive models.

ACKNOWLEDGMENTS

The authors thank Bonnie Antoun, John Korellis and Monica Barney for technical discussions, Jeff Chams for the SEM work, and Tony Chen and Mike Chiesa for program support.

CONTENTS

FIGURES

TABLES

NOMENCLATURE

a	radius of Cu wire
d	diameter of Cu wire
EBSD	Electron Backscatter Diffraction
L_{fiber}	gage length of glass fiber
L_{Cu}	gage length of copper specimen
Q	torque
SEM	scanning electron microscope
κ	twist per unit length
θ_T	rotation (Bionics actuator)
θ_S	rotation (sensor module)
DOE	Department of Energy
SNL	Sandia National Laboratories

1. INTRODUCTION

This is the final report for LDRD project entitled "Size Effects in Continuum Modeling," funded from April, 2008 to September, 2008.

1.1. Background of Size Effects

As the geometrical features in a structure decrease in size (for example in thin films, electronics, micromechanical structures and nanostructures), the mechanical properties of the material have been shown to develop strong dependence on the geometric dimensions, resulting in a size effect, Figure 1. This size effect stems from several competing sources. The geometrical confinement of the material microstructure in a small structure can result in boundary effects, elevated strain gradients, changes in dislocation nucleation and mobility, and an increasing importance of individual grain attributes such as grain size, texture, etc.

Accurate prediction of performance and reliability in micro- and nano-structures requires an understanding of these size effects and employment of physically based micromechanics and/or nanomechanics models that reflect these effects. Conventional continuum mechanics are based on a homogenized material structure, which possess no internal or material length scale. As formulated, no size effects can be predicted by conventional continuum mechanics theories. For example, these theories would conclude that the torque-rotation curves of all copper wires lie on one curve and could not predict the experimental results shown in Figure 1.

Size effects are increasingly being noted and reported in the literature; however, these effects have barely been considered (or included) in the analysis of micro- and nano-systems. The main reasons are the lack of definitive experimental data as well as the added complexity in material modeling. Industrial applications are treated by measuring material properties at the engineering feature size and then applying conventional theories. Development of a predictive capability cannot be based on this kind of ad hoc approach. Several theories have been proposed to model size effects, but have been based on very few experiments conducted at appropriate scales. Thorough studies are necessary to understand and model material deformation at the micron and sub-micron length scale. Consistent sets of experimental data are needed to assess the many theories that have been developed and to validate models that are of sufficient complexity.

1.2. Experimental Evidence of Plasticity Size-Effect

The limited, currently available plasticity size-effect experiments have attracted intense interest of the subject. Some key experiments are briefly described in the following:

1.1.1. Fleck's Torsion and Tension Experiments

The most cited and influential experiment is the tension and torsion of polycrystalline copper wires by Fleck *et al* (1994) [1]. The work is also the most relevant to this investigation. Their experiments were performed on commercially pure, cold drawn copper wires of diameter in the range 12 to 170 μm. All the wires were annealed, giving grain sizes between 5 and 25 μm.

The tension tests were performed on a 50 mm gauge length of copper wire, using a conventional screw driven test machine with a specially designed sensitive load cell, which was a 0.5 mm thick rectangular cantilever beam with strain gauges mounted near the built-in end. For the torsion tests, the copper wire specimen had a gauge length of 2 mm and a 60 mm long glass filament acted as a torsional load cell. The diameter of the glass filament was in the range of 55 to 250 μm to maximize sensitivity of the torsional load cell. A specially designed screw driven torsion machine was used.

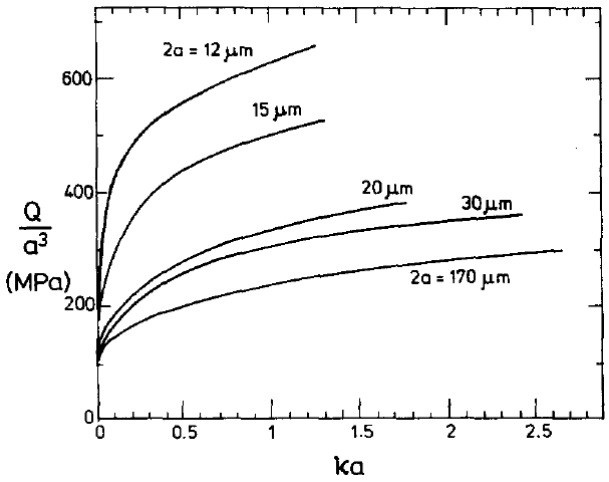

Figure 1 Torsional response of copper wires. Normalized torque-rotation curves show flow stresses rapidly increase as the diameter is reduced. (Fleck et al, 1994 [1])

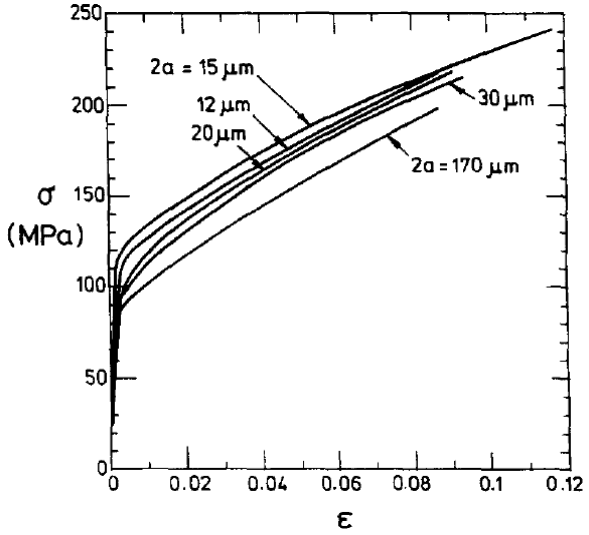

Figure 2 True stress versus logarithmic strain tension data for copper wires of diameter in the range 12-170 μm. There is a negligible effect of wire diameter on the behavior. (Fleck et al, 1994 [1])

The results show decreases in the wire diameter exhibited a negligible effect on the tensile behavior, Figure 2, but displayed systematic increases in the torsional hardening, Figure 1. It implied that size effects are caused by increasing strain gradients and have been used to confirm many strain gradient theories.

1.1.2. Microbend Test

Microbend test was developed by Stolken and Evens (1998) [2]. It involves bending a thin metal foil around a small diameter cylindrical mandrel followed by measuring the unloaded and loaded radii of curvature. By using mandrels having different radii as well as foils with different thicknesses, the plasticity length scale can be established. For annealed high purity (99.994%) Ni foil having thicknesses h= 12.5, 25 and 50 mm and mandrel radii r = 10h, 20h and 40h, the rotational length scale is in the range of 3 – 5 μm, similar to that found previously for Cu using wire torsion tests (Fleck et al, 1994 [1]).

1.1.3. Membrane defection Experiment (MDE)

Another key experiment is the tension of polycrystalline FCC thin films (Au, Al and Cu, thickness from 0.3 to 1.0 μm, average grain size 250 nm) by Espinosa et al (2004) [3]. The MDE technique involves the stretching of a free-standing thin film membrane in a fixed–fixed configuration. A nanoindenter applies a line-load at the center of the span to achieve deflection. It demonstrates a size effect for decreasing film thickness. These experiments were conducted in tension and the specimen was subjected to macroscopic homogeneous axial deformation, i.e. in the absence of any macroscopic strain gradient, in contrast to beam deflection and torsion, where deformation gradients occur.

1.1.3. Micro-compression

Uniform compression of freestanding gold pillars was performed by Greer, Oliver and Nix (2005) [4]. The Au cylinders are created by two fabrication processes, focused ion beam (FIB) machining technique and lithographic patterning and electroplating, and subsequently compressed in the Nanoindenter with a flat punch. The diameter of FIB machined single crystalline <0 0 1>-oriented specimens was in the range of 400 – 7,450 nm. Flows stresses increase significantly for pillars with a diameter of 500 nm and less. For annealed electroplated cylinders having 2 – 3 grains per pillar the significant increase of flow stress occurs at a larger diameter about 1,500 nm. The results also demonstrate that the size effect exists in the absence of strain gradients.

1.3. Size-Effect Issues

These results draw serious concerns and prompt many questions that researchers have anxiously attempted to answer. Does the size effect depend on strain distribution, e.g. uniform versus gradient? How about shear strain versus normal strain and more complex conditions such as biaxial strain? Is size effect the same for different materials? Could there be a size effect purely due to geometry or does it always result from microstructure? Does the continuum approach apply if there are less then five grains through the thickness? More than a decade after Fleck's

monumental wire tension and torsion experiments, the results have not been replicated, why? Even with today's experimental techniques, those are very challenging experiments. The microstructure of the material and experimental procedures were too brief to convince researchers that the result shown in Figure 1 was due to size only but not other experimental or material factors.

1.4. Scope of the Work

The objective of this project is trying to clarify the material and experimental issues surrounding Fleck's work by analytical interrogation and experimentally replicating the historical experiments to corroborate the results. The microstructure of the materials will be controlled so that the geometric parameters will be isolated for investigation. This effort is to understand size effects intended to further develop predictive models.

2. MODELING TENSION THROUGH TORSION

In the experiments of Fleck, data is presented for the uniaxial extension (Figure 2) and torsion (Figure 1) of wires having diameters ranging from 12 μm to 170 μm. Although the uniaxial curves are normally assumed to coincide, both the yield stress and the hardening behavior do vary between wire diameters. In the case of torsion, the variance in the normalized torque is significant. However, can some of the variance in the normalized torque be explained through variance in the tensile response?

We seek to address these concerns through a simplified, analytical approach employing the J_2 theory of plasticity. We bound the hardening behavior in tension through the 15 μm and the 170 μm wires. Note that the 12 μm wire had a slightly lower yield than the 15 μm wire. Because the tensile tests were documented from 0.09 to 0.11 (true strain) and the torsion tests were documented from 1.2 to 2.6 (engineering strain), we will focus on infinitesimal deformations for valid comparison.

To be clear, copper wires of radius a are subjected to a twist β over a length l_0. Often the applied loading is expressed as twist per unit length κ where $\kappa = \beta/l_0$. We can construct a mapping $\mathbf{x} = \chi(\mathbf{X},t)$ to find a measure of true strain in torsion.

$$x_1 = -\kappa t X_2 X_3 + X_1$$
$$x_2 = \kappa t X_1 X_3 + X_2$$
$$x_3 = X_3$$

The velocity **v** is the time derivative of **x**. After writing $\mathbf{v} = \mathbf{v}(\mathbf{x},t)$, we take the gradient to find **L**. We can now find the symmetric part of the velocity gradient **D** and integrate through time to find the true strain in polar coordinates ($z = x_3$) in terms of κ, r, and z.

$$\varepsilon_t = \begin{bmatrix} \frac{\log\left(1+\kappa^2 z^2\right)}{2} & 0 & \frac{\kappa^2 rz}{2\left(1+\kappa^2 z^2\right)} \\ 0 & \frac{\log\left(1+\kappa^2 z^2\right)}{2} & \frac{\kappa r}{2\left(1+\kappa^2 z^2\right)} \\ \frac{\kappa^2 rz}{2\left(1+\kappa^2 z^2\right)} & \frac{\kappa r}{2\left(1+\kappa^2 z^2\right)} & 0 \end{bmatrix}$$

To reduce the kinematics from true strain to engineering strain, we assume κ is small and consequently all terms containing κ^2 are higher order. Consequently, we are left with the familiar relation

$$2\varepsilon_{\theta z} = \gamma_{\theta z} = \kappa r$$

from elementary mechanics. We again note that this exercise only focuses on infinitesimal deformations so that we can employ the tensile data to predict the response in torsion. To this

end the tensile curves in Figure 3 were digitized to provide interpolation functions for relating Mises' stress σ_p to the equivalent plastic strain ε_p.

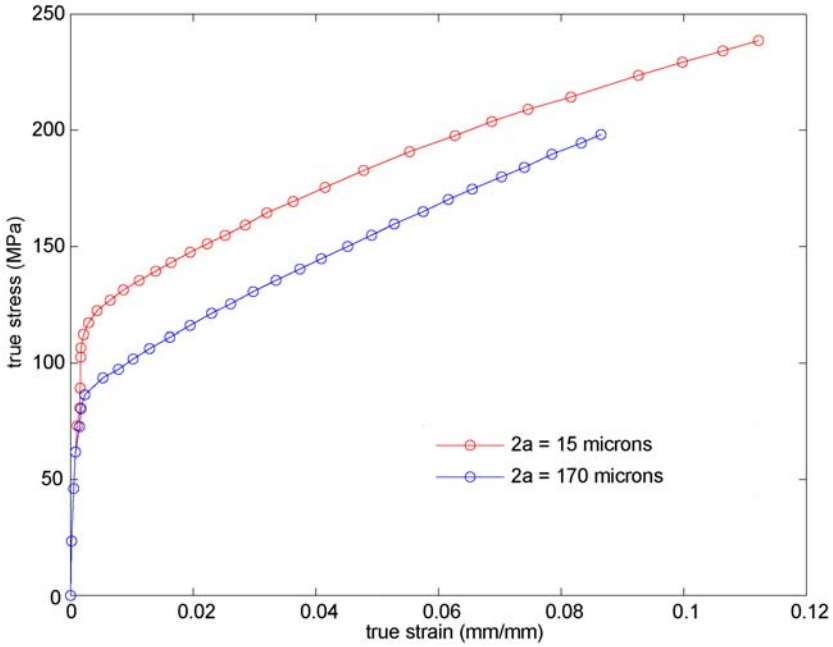

Figure 3 Interpolation functions for the stress-strain response for copper wires of radius *a* in tension. The stress-strain response in tension will be employed to predict the response in torsion.

Given relations for σ_p-ε_p, we can predict the total torque *Q*, derived through an applied κ. We assume the shear modulus μ is 48 GPa and we specify the yield stress in the 15 μm and 170 μm wires to be 103 MPa and 80 MPa, respectively. Given that the shear strain will always vary linearly through the thickness (eg., strain gradient) for both elastic and elastic-plastic responses, we can discretize the wire and integrate through the thickness to find the torque.

We note that in contrast to tension where $\sigma_p = \sigma_{zz}$ and $d\varepsilon_p = d\varepsilon_{p,zz}$, J_2 for torsion stipulates that $\sigma_p = \sqrt{3}/2\sigma_{zz}$ and $d\varepsilon_p = 2/\sqrt{3}d\varepsilon_{p,\theta z}$. Because the load path does not change, we can find the elastic strain $\gamma_{e,\theta z}$ and integrate to find the equivalent plastic strain ε_p at each applied κ. The shear stress $\sigma_{\theta z}$ can be calculated through elasticity $\sigma_{\theta z} = \mu\gamma_{\theta z}$ and J_2 theory (Figure 3). Given the shear stress through the radius *r*, we can integrate the stress acting through a moment arm *r* to find the total torque

$$Q = \int_0^a \int_0^{2\pi} (\sigma_{\theta z} r) r dr d\theta$$

and normalize that torque by the radius of the wire cubed a^3. Through this normalization, we can compare with the experimental findings noted in Figure 1. Both the experimental findings and the predicted results are illustrated in Figure 4. Because the tension data was bounded, the torsion data is also bounded. In this case, the smallest wire diameter, 12 μm, is the upper bound.

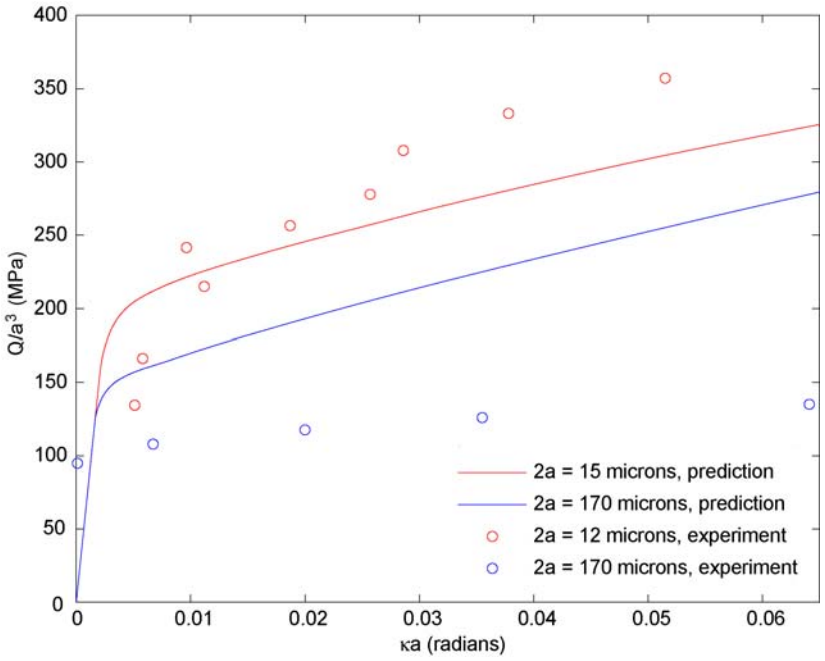

Figure 4 Comparison between measured and predicted values of the torque Q for an applied twist per unit length κ for varying wires of radius a. Although the predicted results do not coincide with measured values, small changes in the hardening behavior are amplified in the normalized torsion response.

As noted in the Figure 4, the predicted values do not match measured values. The simplified analysis, however, does shed light on a few issues. We will first assume the 170 μm to be "macroscopic." Barring size effects, J_2 theory does not appear adequate to predict the response in torsion. We can only speculate as to the cause of the anisotropy, but it may suggest that the microstructure has been altered through processing. That alteration may or may not enhance the measured size effect. We also note the obvious. The independent variable in Figure 4 is the engineering shear stain at the outer radius of the wire. We can compare at a common equivalent plastic strain (neglecting elasticity) and find that a 30 MPa difference in Figure 3 translates into a 53 MPa difference in Figure 4. The chosen scaling for torsion amplifies differences in the tensile response. Again, this amplification cannot explain the differences in torsion but the simplified analysis does yield a measure of that amplification.

This simplified study illustrates that variances in the tensile response are amplified in the torsion response. In the study of size effects, caution should be applied to note those differences and provide a statistical representation of the measured response. Provided one can show that the response is not a function of the microstructure, simple exercises such as mapping tension into the torsion can further justify the measured size effect.

3. MATERIAL

3.1 Copper wire

Commercially available copper wires 99.99% pure, cold drawn and annealed, were selected for this study. Five different sizes were obtained, nominally, 0.007, 0.0012, 0.0008, 0.0006, and 0.0005 inch diameter (i.e. 180, 30, 20, 15, and 12 μm, the same sizes as those in Fleck's experiments, 1994); they were identified as w007, w0012, w0008, w0006 and w0005, respectively. W0005 is the thinnest wire obtainable from the source [5]. Wires were tested under the as-received condition.

After polishing and etching, the wire samples were subjected to microscopic examination. The optical micrographs of these wires are shown in Figure 5 - Figure 9. It was difficult to align thin wires in the mold. The polished surface generally appeared in elliptical shape rather than circular, which indicated that the cross section shown was not normal to the axis of the wire. The minor radius of the ellipse, however, is the radius of the wire. The actual wire diameter was determined from micrographs by averaging at least four measurements from different cross sections of the same size. The size of digital micrograph is 2048x2048 pixels. The resolution of measurement is about 0.2 μm. The measured diameter is listed in Table 1.

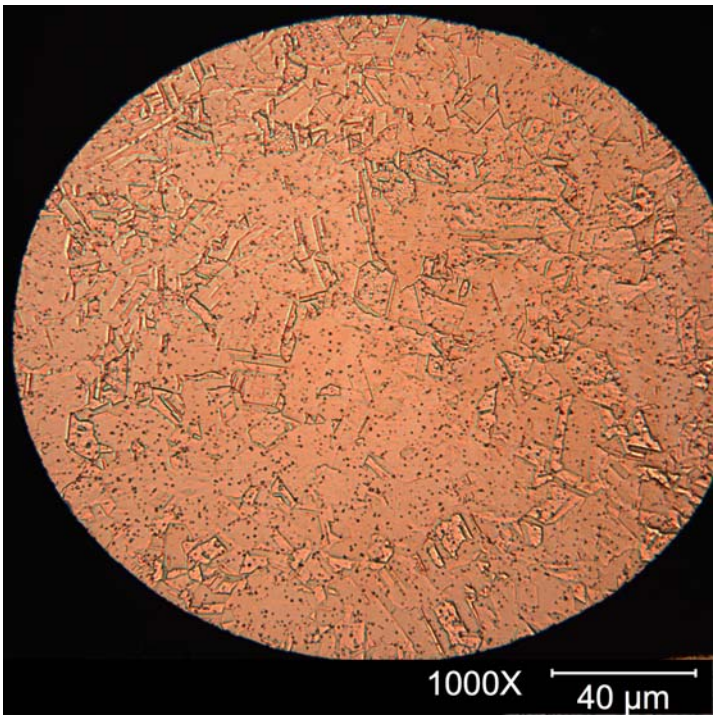

Figure 5 Optical micrograph of w007 (180 μm) Cu wire.

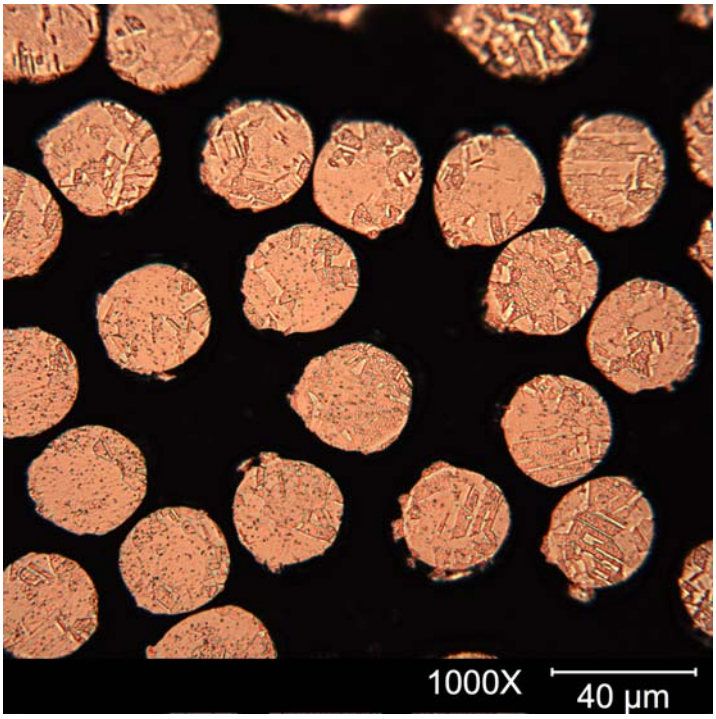

Figure 6 Optical micrograph of w0012 (30 µm) Cu wire

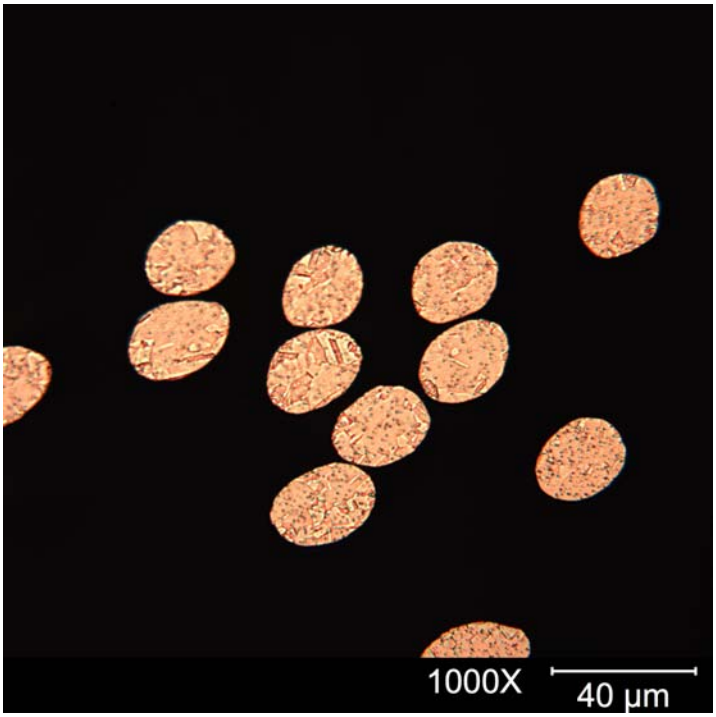

Figure 7 micrograph of w0008 (20 µm) Cu wire.

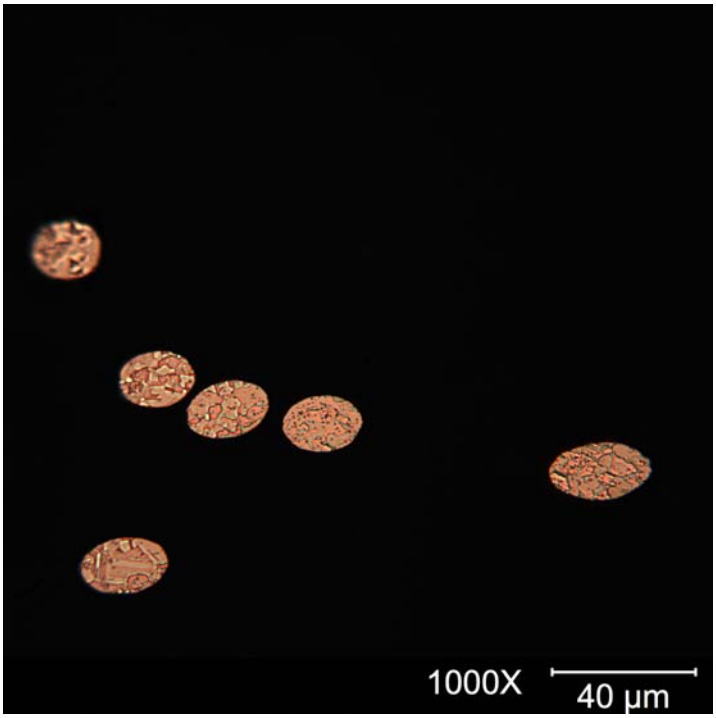

Figure 8 micrograph of w006 (15 µm) Cu wire

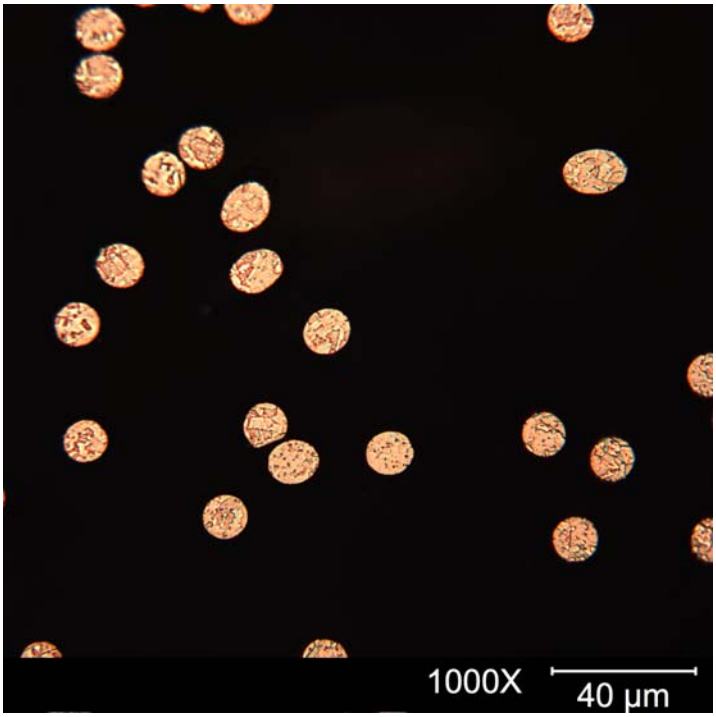

Figure 9 micrograph of w005 (12 µm) Cu wire

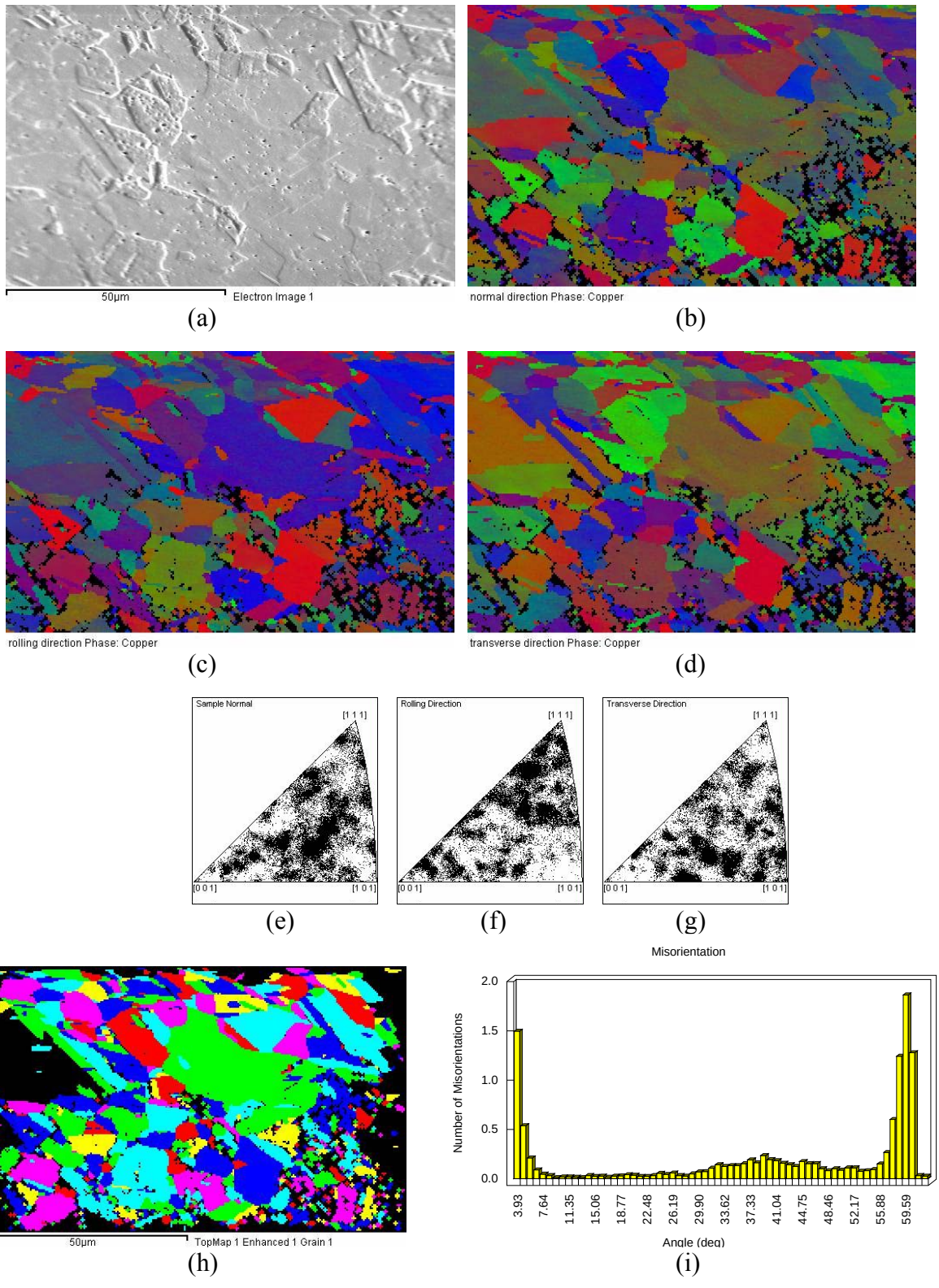

Figure 10 EBSD results of size 0.007 inch wire. (a) forward scattered electron image, (b)(c)(d) Crystal orientation maps in normal, rolling and transverse direction, (e)(f)(g) corresponding inverse pole figures, (h) enhanced color map showing grain positions, (i) Histogram of misorientation angles

Table 1 Copper Wire Diameter

Wire	w007	w0012	w0008	w0006	w0005
Diameter, μm	179.0	29.9	20.8	15.6	12.0

3.2 EBSD crystallographic analysis

It is well know that grain size and texture affect the mechanical behavior of the metal. A consistent microstructure is important in this study. The optical micrograph reveals the microstructural information of a sample such as grain size, deformation mechanism, etc. To obtain quantitative crystallographic information of wires, Electron Backscatter Diffraction (EBSD) technique was used to examine these samples in the scanning electron microscope (SEM). Three wire sizes were involved: w007, w0012 and w0005.

Figure 10 displays EBSD data of w007 and the microstructural information after processing the data. Figure (a) is a forward scattered electron image. It indicates the scanned area of EBSD analysis. Crystal orientation maps shown in (b) – (d) are based on the samples normal, rolling and transverse directions, respectively, which reveal the positions of all grains and grain boundaries in the sample microstructure. (The Sample configuration and orientation color code for the maps are depicted in Figure 11.) The corresponding inverse pole figures are shown in (e) – (g). It appears there is no clear preferred crystal orientations (texture) presented in the material. The enhanced color map showing grain positions is displayed in (h), where the distribution of grain sizes can be measured. All neighboring points within a grain have a misorientation less than 5°. The distribution of grain boundary misorientation angles is shown in (i). A large number of misorientation at high angles implies many twins in the microstructure. The average grain size calculated is 7.3 μm. The number may be underestimating because there are many twins present. The largest grain shown is about 40 μm.

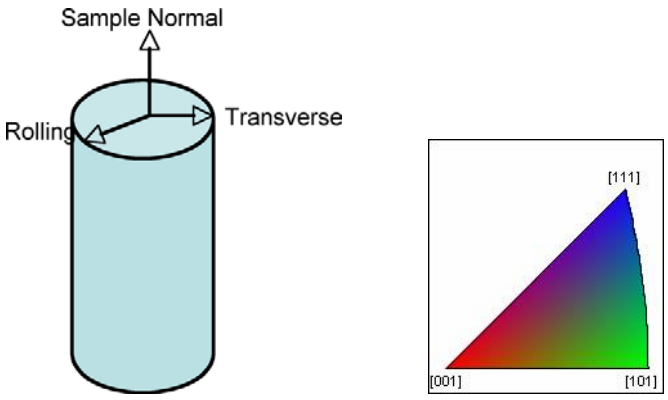

Figure 11 Sample configuration (left) and orientation color code for the maps (right).

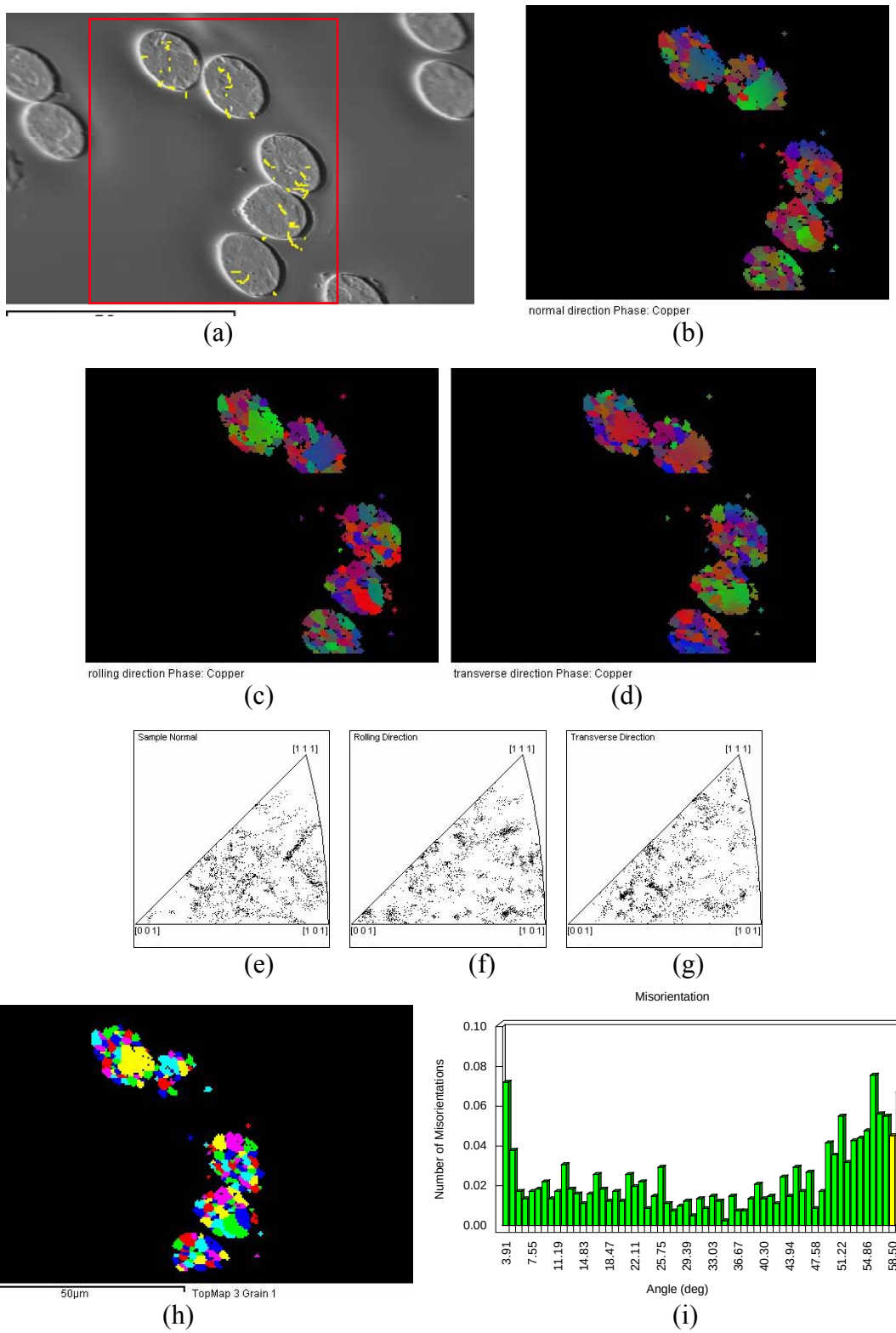

(a) (b) (c) (d) (e) (f) (g) (h) (i)

Figure 12 EBSD results of size 0.0005 inch wire. (a) forward scattered electron image, (b)(c)(d) Crystal orientation maps in normal, rolling and transverse direction, (e)(f)(g) corresponding inverse pole figures, (h) enhanced color map showing grain positions, (i) Histogram of misorientation angles

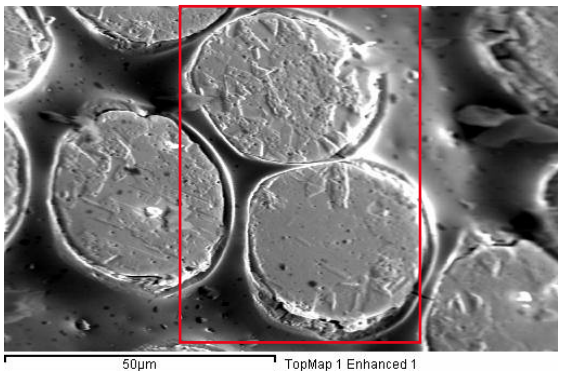

(a)

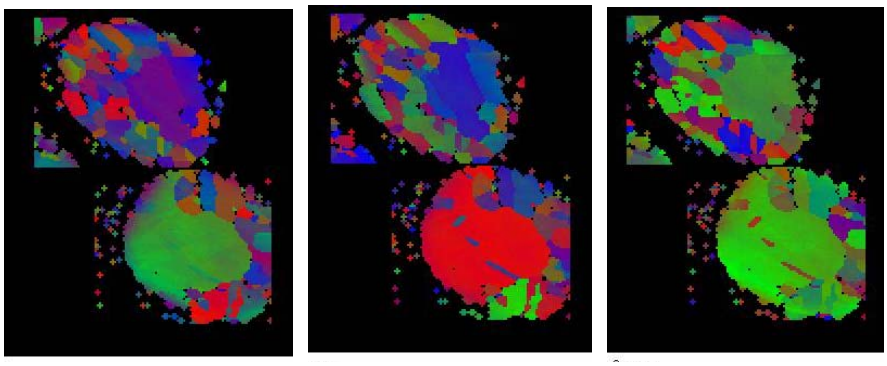

(b) (c) (d)

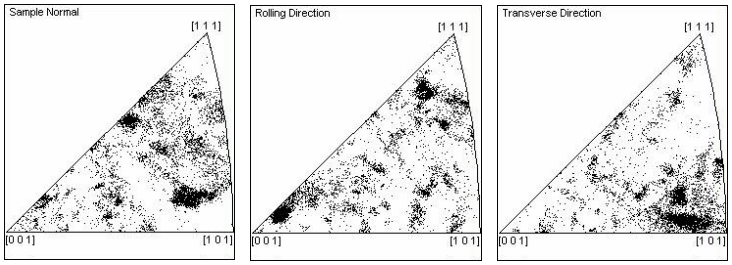

(e) (f) (g)

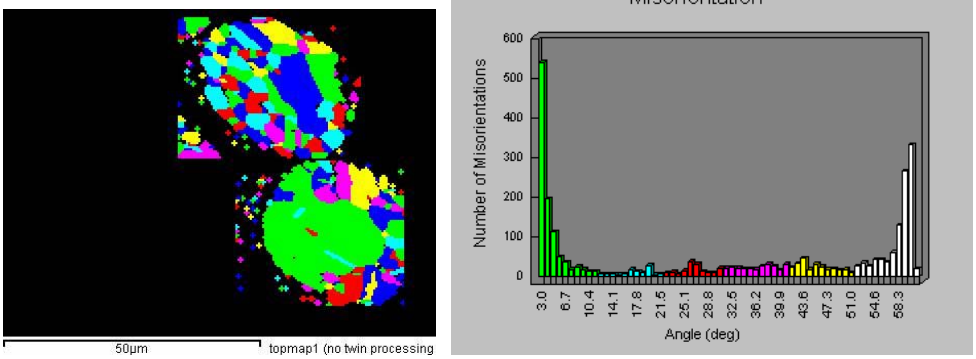

(h) (i)

Figure 13 EBSD results of size 0.0012 inch wire. (a) forward scattered electron image, (b)(c)(d) Crystal orientation maps in normal, rolling and transverse direction, (e)(f)(g) corresponding inverse pole figures, (h) enhanced color map showing grain positions, (i) Histogram of misorientation angles

Similarly, results of EBSD analysis of w0005 and w0012 are shown in Figure 12 and Figure 13, respectively. The microstructures of these wires are quite similar, many annealing twins but no significant texture present. The average grain size and the largest grain observed are summarized in Table 2. Clearly, larger size wire has larger grain size. The average grain size of all wires is at the same order of magnitude. Although there are many grains identified for a cross section (even the smallest size wire has at least 30 grains), the variation in grain size is quite large. Grains having the size of the radius of the wire are commonly observed except w007.

Table 2 Grain size

Wire diameter, μm	180	30	12
Average grain size, μm	7.3	6.4	3.2
Largest grain size, μm	40	15	7

3.3 Equiaxed grain

The copper wires had been cold drawn before annealing. The grain shape could be elongated in the axial direction. Wire samples of the largest (180 μm) and a smaller (15 μm) sizes were mounted longitudinally in separate molds, then polished and etched for optical microscopic examination. The initial intent was to examine the smallest size (12 μm). Due to the difficulty of handling the thin wire, the second smallest was studied. Figure 14 and Figure 15 show that grains are not elongated in both w007 and w0006 wires. This implies the wires have equiaxed grains. The micrograph of the 180 μm wire (Figure 15) also demonstrates that the large grains are located close to the center of the wire and the small grains are tend to be near the surface.

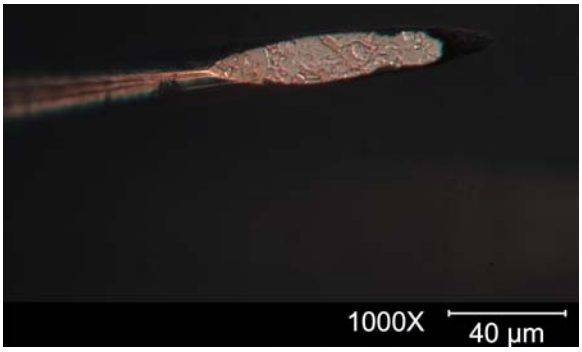

Figure 14 Optical micrograph of w0006 (15 μm wire) showing longitudinal direction.

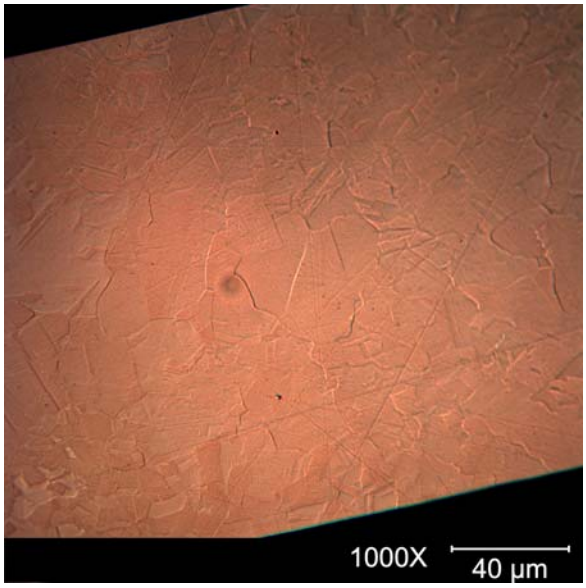

Figure 15 Optical micrograph of w007 inch wire showing longitudinal direction.

4. TENSION EXPERIMENT

4.1 Tension Experimental Setup

To obtain tensile stress-strain curves of small copper wires, the applied tensile force and the elongation of the gage section need to be measured accurately. Estimated from the experiment of Fleck *et al*. [1], the tensile yield stress for annealed copper wires is about 100 MPa (Figure 2). Based on this value, the loads needed to yield various Cu wires are listed in Table 3. The load range spreads over two orders of magnitude. It required two testing systems with different load measuring capacity to run the tests and acquire data with the best resolution. One was MTS858 Bionics System for testing w007, the other was Bose ElectroForce TestBench System for smaller size wires. Although the applied load was very small, commercial available load cells were adequate for the work.

Table 3 Estimated yield load of copper wire

Wire	w007	w0012	w0008	w0006	w0005
Force at 100 Mpa, N	2.517	0.070	0.034	0.019	0.011

4.1.1 Setup on Bionics

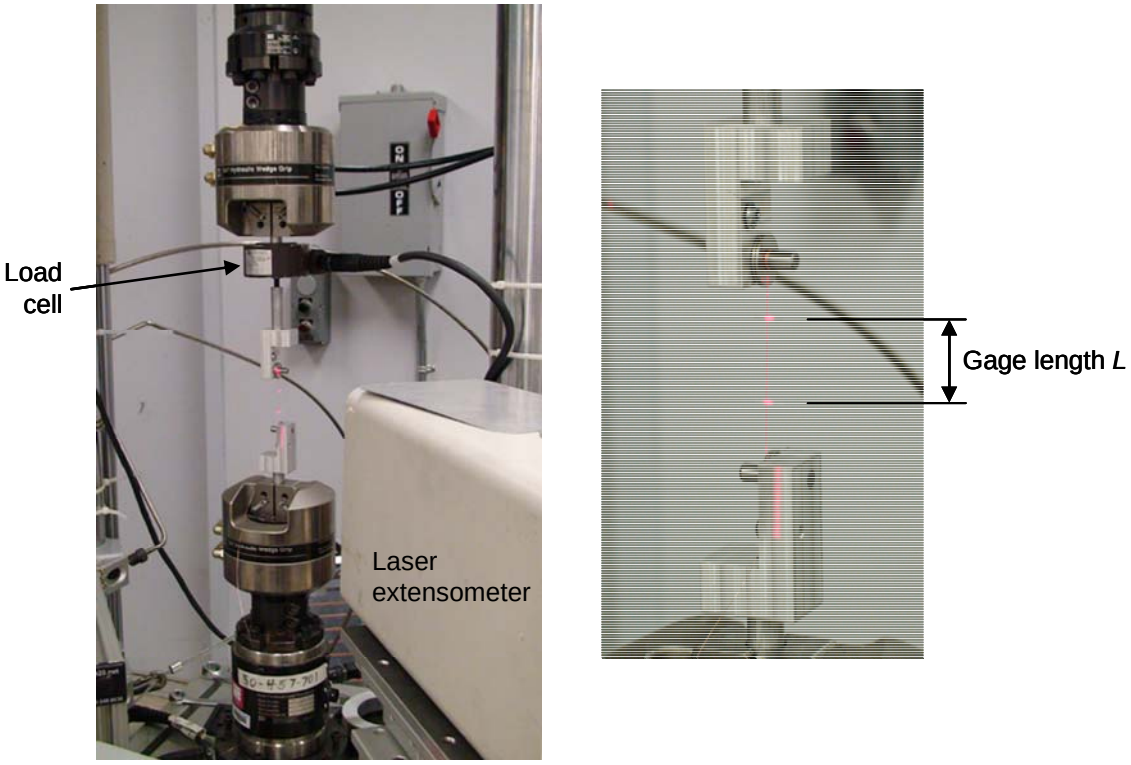

Figure 16 Tensile experimental setup for w007 (180 μm) Cu wire

Figure 16 shows the experimental setup on the Bionics. The system load cell was 15 kN, which did not have enough resolution for the small load, so a 100 N load cell was adapted in the loading chain to measure the load.

Thin wire is difficult to grip. It may slip in the fixture or have stress concentration near the fixture, which will cause erroneous elongation measurement from the actuator displacement. To circumvent this problem, two micro-balloon reflecting tapes were stuck on the wire at some distance away from the fixture to mark the gage section. The elongation of the gage section was measured by using a laser extensometer. Furthermore, a pair of anti-slip stress-concentration-free fixtures was designed (Figure 16, right), which worked well and could load the wire to a very large strain.

4.1.2 Setup on TestBench system

Figure 17 illustrates the setup on TestBench, which utilizes a 100 g load cell. Similar to the setup on Bionics, laser extensometer was used to measure the elongation of a gage section.

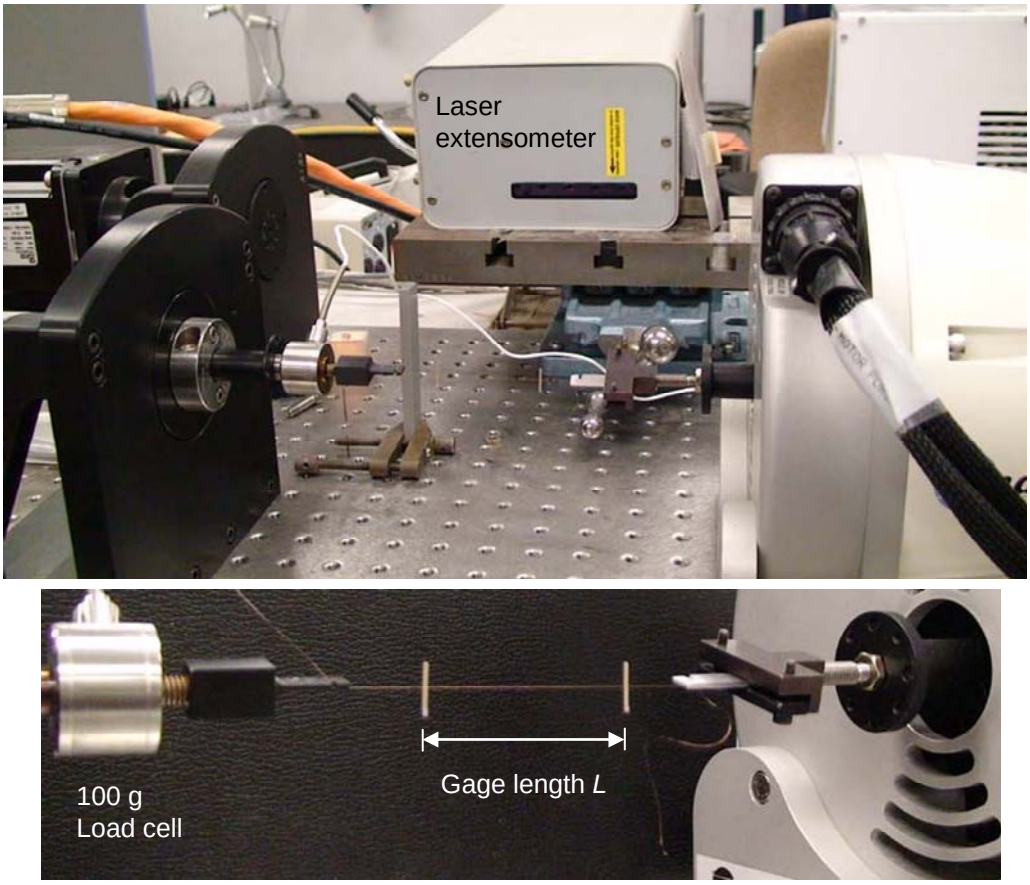

Figure 17 Tensile experimental setup for Cu wires equal or smaller than 30 μm.

4.2 Experimental results

The tensile tests conducted are listed in Table 4. At least two repeats for each size are included. Both setups worked very well. Since the laser targets were applied manually, the gage length varied from test to test. The engineering stress-strain curves of each size are plotted in Figure 18 to Figure 22.

Table 4 Tensile test matrix

Cu wire	Frame	Specimen No	Gage length mm
w007	Bionics	8	26.26
		9	26.00
w0012	TestBench	1	46.05
		5	42.39
w0008	TestBench	3	41.61
		4	44.32
		5	45.33
w0006	TestBench	1	46.92
		2	50.72
		3	43.83
w0005	TestBench	1	51.70
		4	46.04

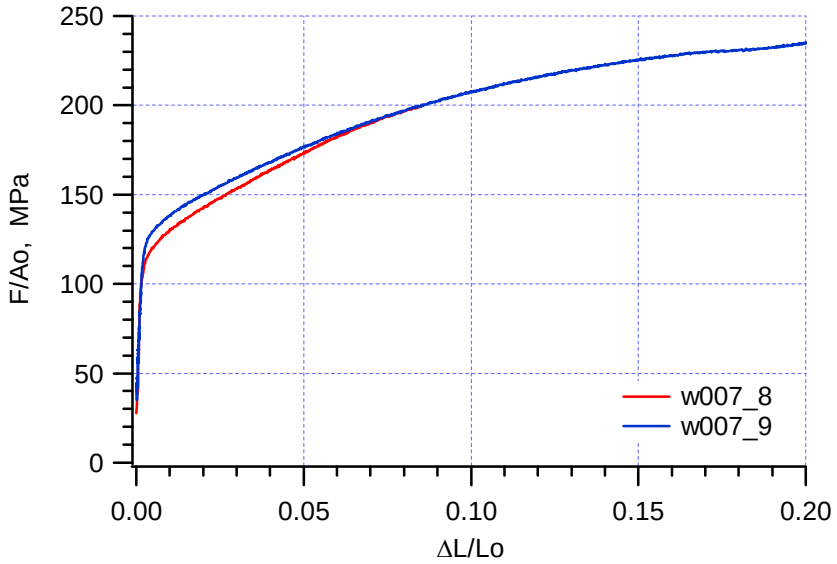

Figure 18 Tensile stress-strain curves of w007 (180 μm) Cu wire

The curves of w007 specimens, shown in Figure 18, are very clean signals. The transition from elastic to plastic deformation is gradual. The yield stresses of w007_ 8 is about 110 MPa, which is slightly lower than that of w007_9 at 125 MPa. Specimen w007_ 8 displays a higher hardening rate.

Figure 19 shows the results of two w0012 specimens. This is the largest size of wire tested on TestBench configuration. Signals are clean but involve some random noise, which can be removed by signal processing. A smoothed curve of w0012_1 data is also plotted in the figure. Both specimens have very consistent deformation behavior - yield at 165 MPa and the same hardening rate.

As the size of the wire becomes smaller, it appears the stress-strain curve becomes noisier. This is because the noise level of a setup is fixed and the magnitude of the load signal is proportional to the cross sectional area of the specimen. The signal-to-noise ratio degrades as the wire decreases in size .

For the next smaller size w0008, the results are not as consistent as w0012. The yield occurred at 125, 140 and 145 MPa for three w008 specimens (Figure 20). Similar results are observed in size w0006 specimens. The scatter of yield stress is even worse having values of 130, 190 and 200 MPa (Figure 21). Variation in hardening rate is also observed within the same size group; it appears that those specimens having a lower yield stress always have a higher hardening rate.

The stress-strain curves of the smallest size w0005 specimens are shown in Figure 22. The yield stress values are 160 and 180 MPa. In this set of test, the maximum force reached was less than 25 mN.

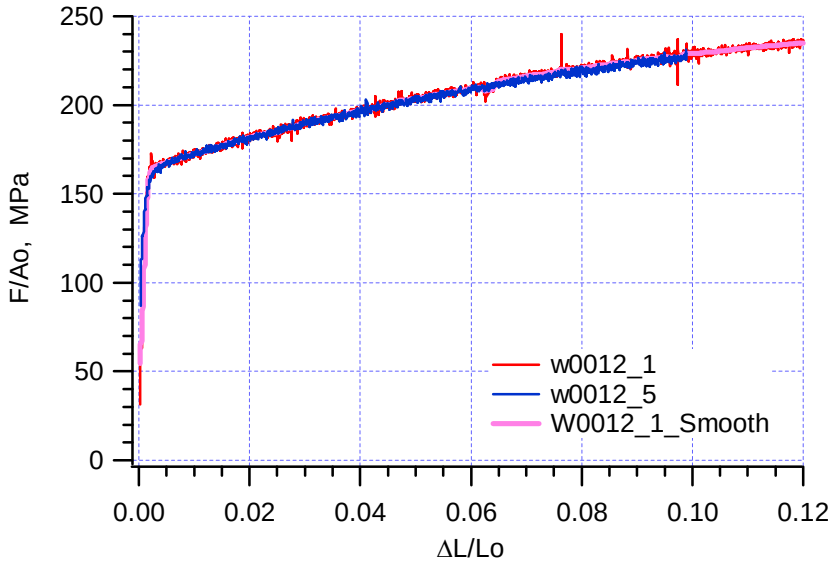

Figure 19 Tensile stress-strain curves of w0012 (30 μm) Cu wire

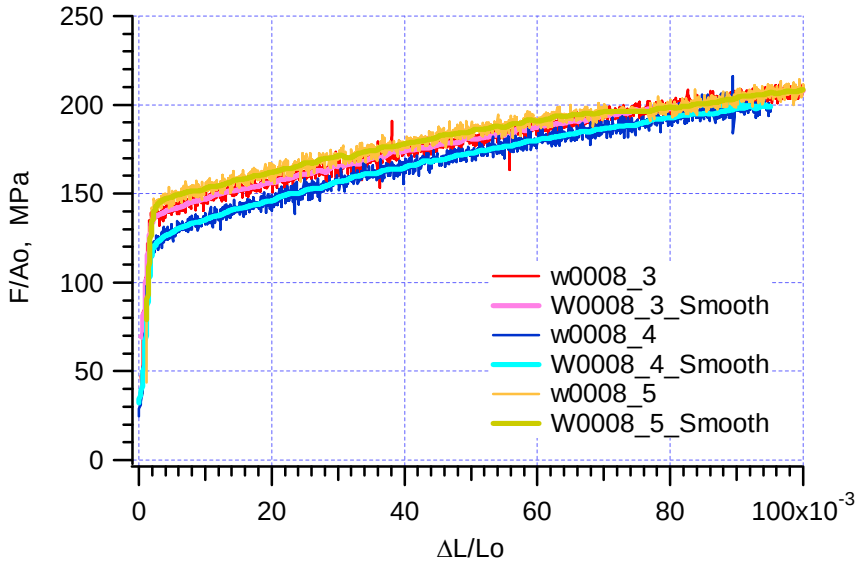

Figure 20 Tensile stress-strain curves of w0008 (20 μm) Cu wire

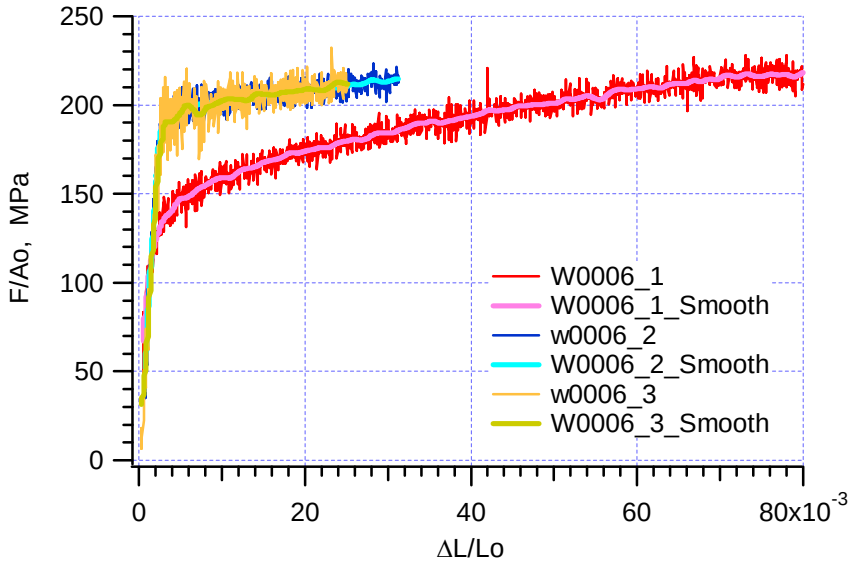

Figure 21 Tensile stress-strain curves of w0006 (15 μm) Cu wire

4.3 Discussion

4.3.1 Handling

Successful experiments are presented in the last section. Not reported are many failed attempts especially in the initial stage of experimentation. Handling thin wires is difficult. They are barely visible with the naked eye, hard to grip, easy to break and deform plastically. Since

plasticity is path dependent, previous deformation history will affect the deformation during loading, which shows up in the stress-strain curve such as yielding and hardening behaviors. It may also cause undesired wire rotation during tension for which the rotating laser target on the wire will generate additional error in measuring elongation. Aligning the laser beam right at the wire could reduce the error due to rotating tapes, but the issue of how to quantify the plastic deformation or avoid it during handling is extremely challenging. Special attention had been paid to minimize the plastic deformation during mounting. This issue may be resolved by building a special device to help mounting thin wire specimens, but it requires time and resources beyond the scope of this project.

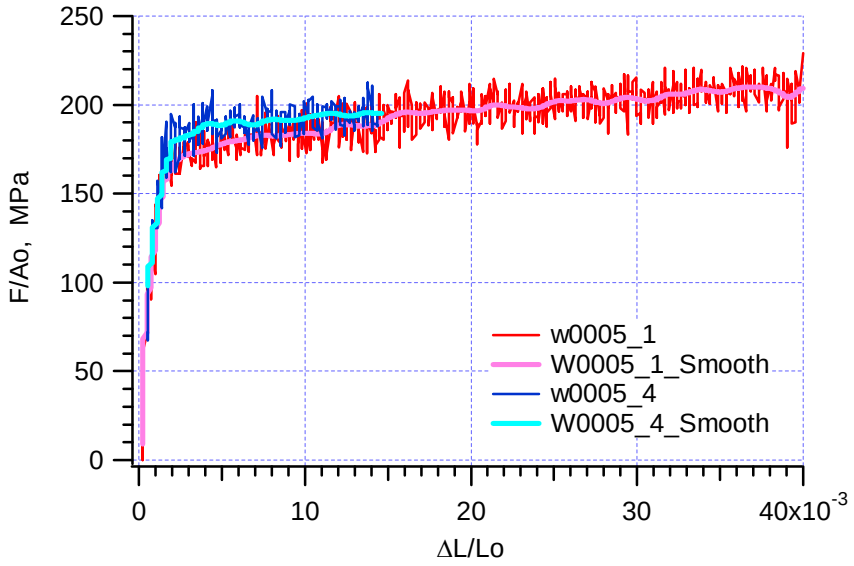

Figure 22 Tensile stress-strain curves of w0005 (12 μm) Cu wire

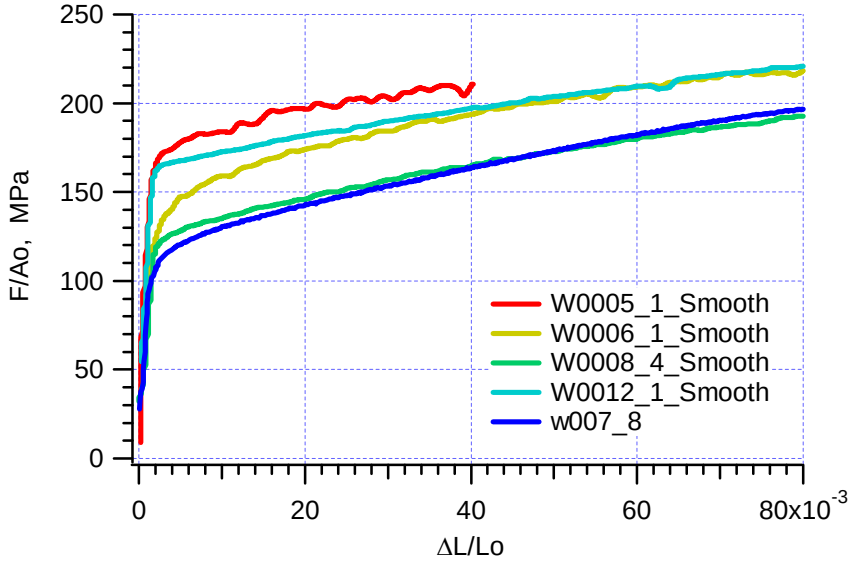

Figure 23 Summary of tensile stress-strain curves

4.3.2 Yielding and hardening

From repeated measurements, the yield stress is quite consistent in some size (e.g. w0012) and scattered in others. Since the load is very small, a slightly offset load signal can easily change the yield stress by 10 – 20% or larger. To make sure an accurate offset value was recorded, the wire specimen was cut into two pieces before the end of loading program if it was not already broken by tensile load, so a zero load condition could be clearly established and the offset was subtracted from the load signal.

If the specimen size is the same, the material is consistent, and the measurement is accurate, what contributes to the large scattering of yield stress? A very possible reason is the uncounted plastic deformation before testing. The specimen having higher yield stress had experienced a larger load before test. The pre-experiment plastic deformation can also explain the observed phenomenon that a higher hardening rate corresponds to a lower yield stress since hardening rate typically decreases as plastic strain increases. Based on this theory, the specimen with the lowest yield stress in the group was the one had the least pre-experiment plastic deformation. It is selected to represent the group and make comparison with the other sizes. Those selected curves are plotted in Figure 23.

Based on the similarity of the hardening behavior, the curves can be grouped into two sets,. The first set includes w007, w0006, and w0005. W0012 and w008 are the second set. The yield stresses are all different. In the first set, the smaller size wire has the higher yield stress; however, the trend is different in the second set. The yield-hardening phenomenon observed within the same size is not applicable when different sizes are considered.

4.3.3 Summary

Tensile experiments of very thin copper wires were carefully performed and their stress-strain behaviors were characterized successfully. Obviously, more repetitions are needed to bolster the results. Wires in the first set including w007, w0006 and w0005 are better candidates for size effect studies since they have similar hardening behavior and a consistent relation of size verse yield stress. It would be easier to compare the behavior of these wires under different loading condition such as torsion.

5. TORSION EXPERIMENT

5.1 Torsion Experimental setup

Two torsional setups were needed for this investigation. A single system did not have either the sensitivity or the capacity to test Cu wires or calibrate glass fibers. The first setup was based on the MTS Torsionmaster System and Nano17 Six Axis Force/Torque Sensor [6]. It has a large torque capacity but limited resolution. The second custom setup has a higher resolution but lower capacity. It basically followed the concept in Fleck's paper [1] by hand building a rotation sensor and using a glass fiber for torque measurement. Both systems are described in the following.

5.1.1 Torsionmaster and Nano17

Nano17 is one the most sensitive torque sensors that are commercially available. It is a six-axis force/torque sensor, which measures three force components, *Fx, Fy, Fz,* and three torque componsnts *Tx, Ty, Tz*. In this application, only *Tz* is of interest. According to the specification, the sensor has a torque range of ± 120 N-mm and a resolution of 1/64 N-mm. As shown in Figure 24, the sensor is mounted on the left chuck of the MTS system, which does not rotate but can be adjusted for fixed axial position or floating by applying a constant tensile force. The right chuck is connected to the rotation actuator. The MTS system provides accurate rotation control and measurement as well as precise specimen alignment.

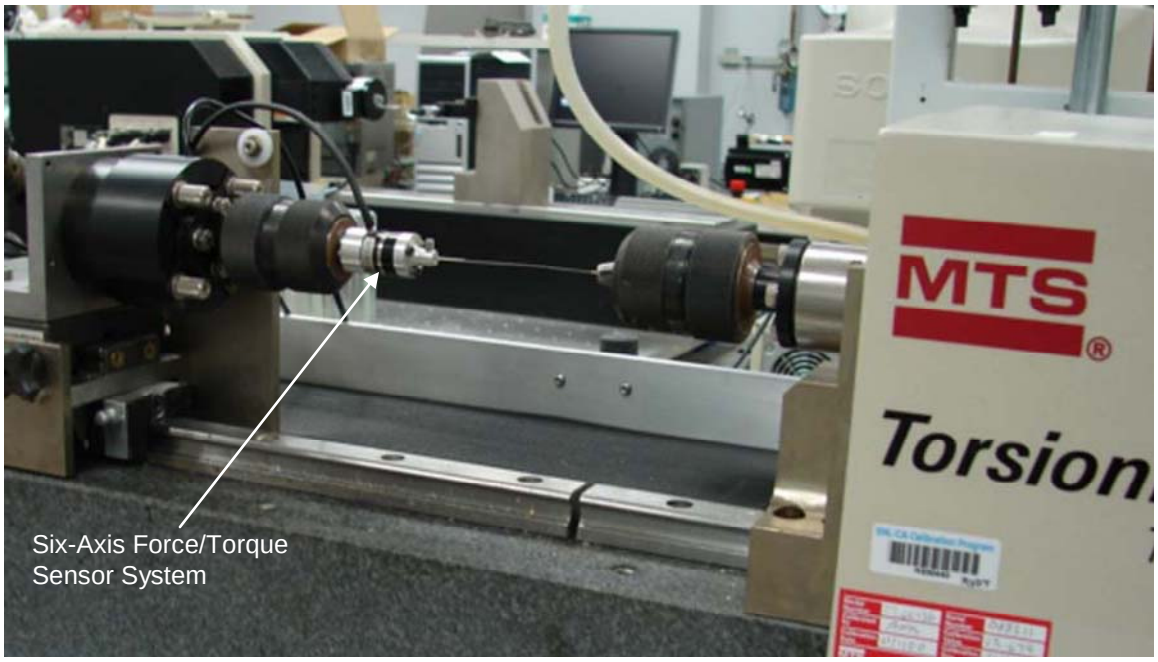

Figure 24 Torsion experimental setup of 0.007 inch (180 μm) Cu wire

5.1.2 Bionics and the customized module

The setup is built on the MTS858 (Bionics) Axial-torsional System as shown in Figure 25, which utilizes the system's vertical configuration, rotation control and measurement, and data acquisition. The custom made loading and sensing module, shown in Figure 26, includes the following components, from top: fiber optics connector, ferrule, glass fiber, laser rotation sensor, specimen (Cu wire), weight, and rotation constraining fixture. The module is connected to the Bionics system rigidly through hydraulic grips. The axial-torsional actuator is on the top. During the experiment, the axial channel is inactive and the torsional channel is under rotation control. The top of the module is subjected to an angular displacement θ_T. The fixture at the bottom of the module shaped like an open channel, is fixed to the MTS frame at the bottom and houses the weight at the top. The weight is allowed to move freely in the axial direction, but the rotation is constrained by the channel walls, i.e. $\theta_B = 0$.

The mid-section of the module is the laser rotation sensor. A reflective tape is attached diagonally on a rectangular paper. The paper is then wrapped around a foam cylinder, which has a small diameter steel tube at its center axis. The wrapped reflective tape forms a helix in space. Combined with another reference tape bonded on the shaft of the actuator, it can precisely convert the angle of rotation θ_S to linear displacement Δh that is measurable by a linear laser extensometer

$$\theta_S = c_1 \, \Delta h$$

where c is a conversion coefficient.

The glass fiber acts as a torque sensor. Here a single-mode fiber optical cable is used. To ensure the fiber is linear elastic, the outer plastic buffer coating of the cable needs to be stripped and leaves only glass core and cladding for the application. A stripped fiber is shown in Figure 27, which has a nominal diameter of 125 μm. The fiber runs through and is firmly attached to the ferrule on the top and the steel tube at the bottom using M-bond 200 adhesive. Similarly, the wire specimen is attached to the lower side of the laser rotation sensor through the steel tube and has a weight hanging below.

In the setup all components can be considered rigid except the specimen and the glass fiber. The rotations at the bottom end of the glass fiber, the top end of the Cu wire, and the laser rotation sensor all have the same angle θ_S. If the specimen and the glass fiber have the gage lengths of L_S and L_G, respectively, the twist per unit length of the specimen κ_S and the glass fiber κ_G are:

$$\kappa_S = \theta_S / L_S \quad \text{and} \quad \kappa_G = (\theta_T - \theta_S) / L_G$$

Since θ_T is the applied rotation, which is known, by measuring the angle θ_s, which is the deformation of the copper specimen, the rotation of the glass fiber ($\theta_T - \theta_S$) is determined. The applied torque Q is linearly related to the rotation of the glass fiber by

$$Q = c_2 \, \kappa_{G.}$$

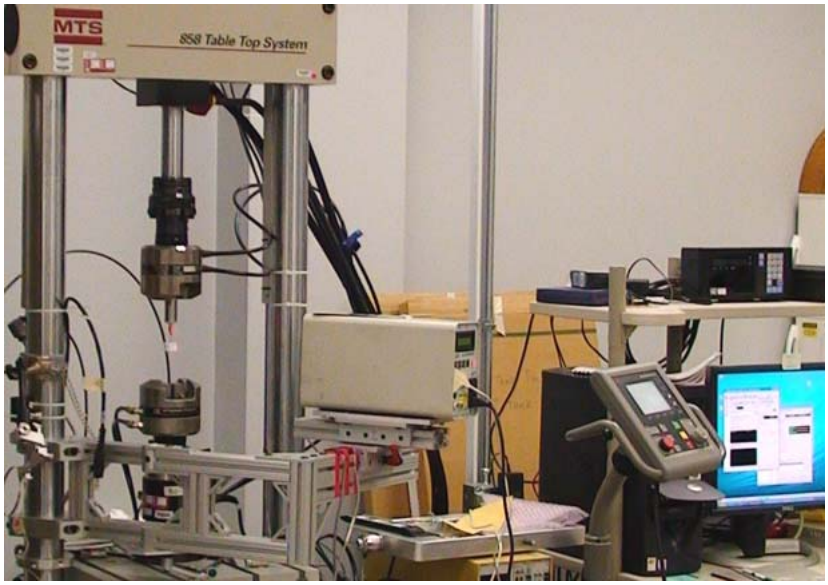

Figure 25 Torsion experimental setup of small diameter specimen.

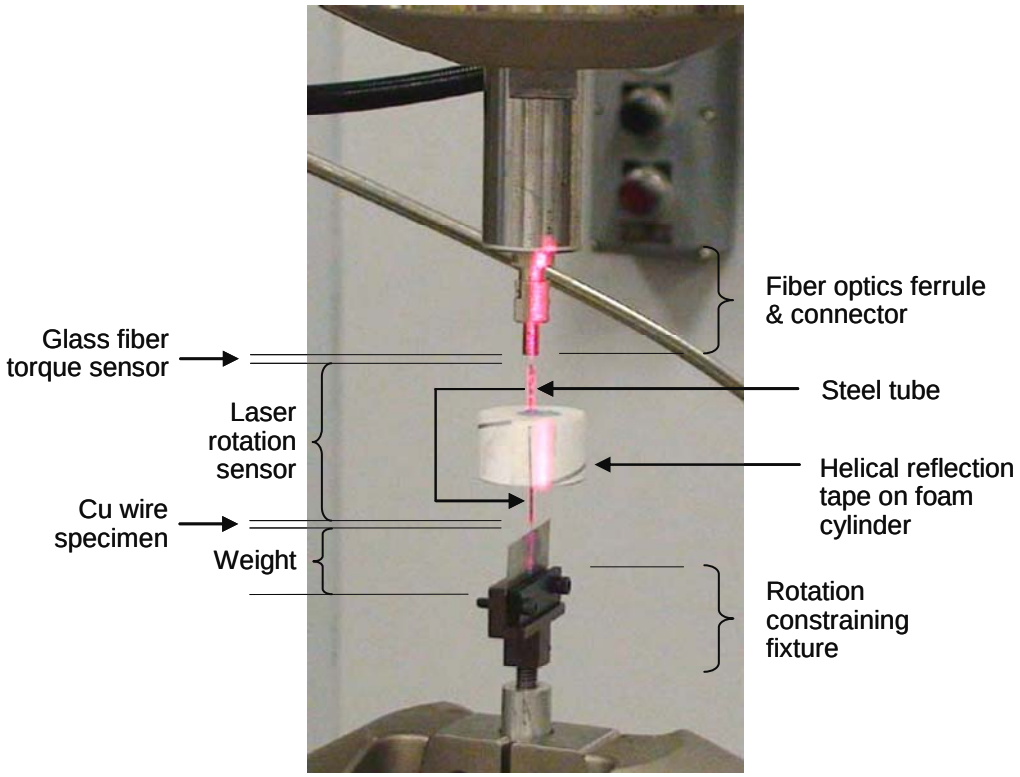

Figure 26 Torque and rotation measurement.

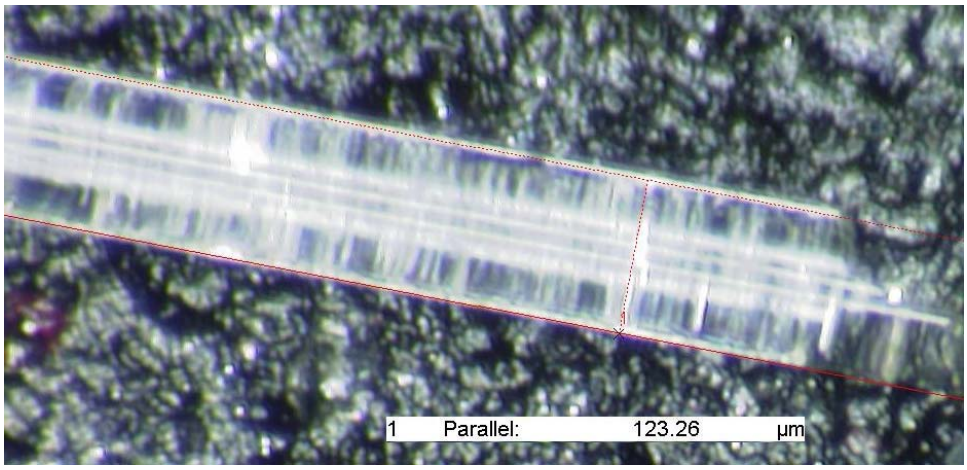

Figure 27 Glass fiber dimension viewing under Keyence measuring microscope.

5.2 Calibration

The torque and rotation sensors in the customized module of the Bionics setup are not standard commercial items. Calibrations of parameters c_1 of the rotation sensor and c_2 of the glass fiber are required.

5.2.1 Glass fiber

Short steel tubes, about 0.5 mm diameter and 10 - 15 mm long, were adhered to both ends of a fiber optics cable so it could be clamped in the Torsionmaster system without damaging the fiber as shown in Figure 24. The calibration test was repeated several times using different specimens as listed in Table 5.

Table 5 Calibration of glass fiber

Specimen	Length mm	Stiffness N-mm^2/degree
fiber02	50.8	0.0151
fiber03	55.6	0.0132
fiber04	50.0	0.0129
fiber05	25.4	0.0128
fiber06	26.2	0.0123
fiber07	25.4	0.0127
max		0.0136
min		0.0110

A typical normalized torque-rotation relation of the glass fiber is displayed in Figure 28. Science the torque is very small, even the most sensitive torque cell appears to be very noisy. The data, although scattered, shows a clear trend of linear relationship between the torque and rotation. A line is fitted through the data. The slope of the line is also reported in Table 5. The fitted lines of all calibration runs are summarized in Figure 29.

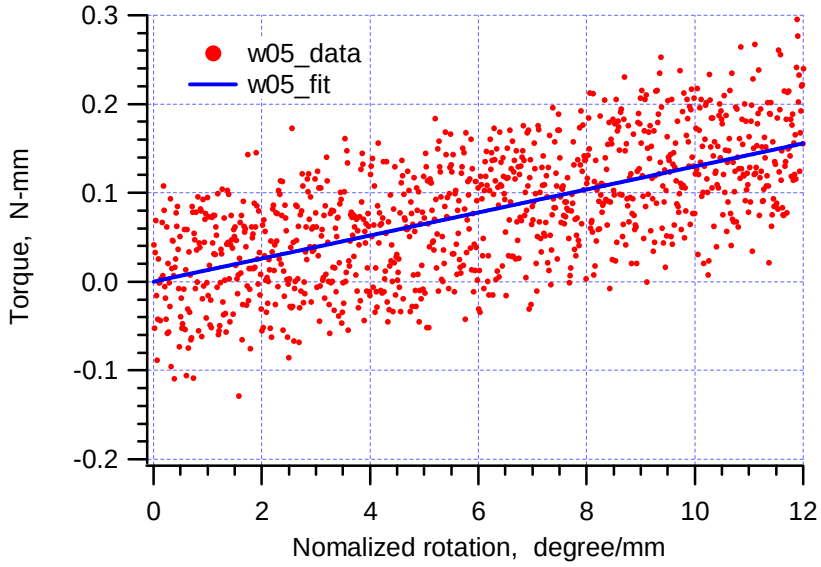

Figure 28 Typical results of glass fiber calibration, Specimen fiber05.

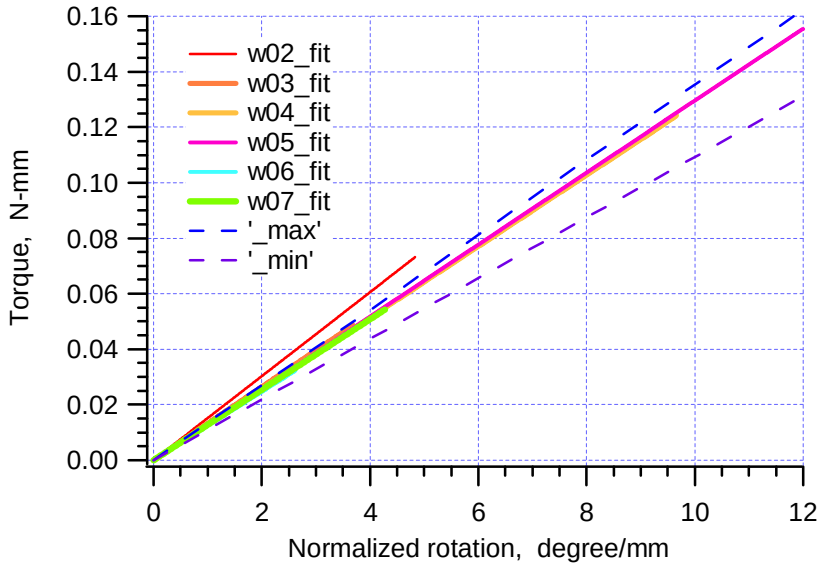

Figure 29 Measured torsional stiffness of glass fiber.

The shear modulus G of glass is typically within the range of 26.2 – 32.4 GPa. Using these values to calculate the property of a glass fiber, the torsional stiffness has the maximum and minimum values of 0.0136 and 0.0110 N-mm-(degree/mm)$^{-1}$. The lines predicted with the maximum and minimum slopes are shown in blue lines in Figure 29. Except specimen fiber02 all results are within the range. The averaged value of all slopes is 0.0132 N-mm-(degree/mm)$^{-1}$.

5.2.2 Laser rotation sensor

If there are no specimen and weight attached, the laser rotation sensor is free to rotate. The sensor angle will be the same as the actuator angle, $\theta_S = \theta_T$. This configuration was used to calibrate the laser rotation sensor. A typical calibration curve of the laser extensometer output voltage versus the rotation angle is shown in Figure 30.

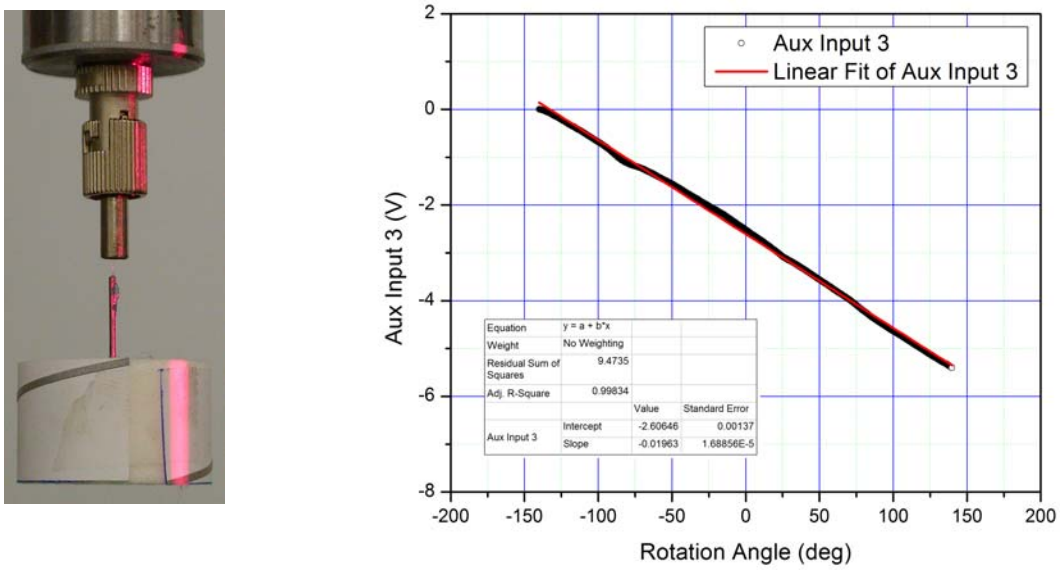

Figure 30 Calibration of the laser rotation sensor.

5.3 Experiments

From the data shown in Figure 1, the yield condition for copper wire is approximately at Q/a^3 = 150 MPa. Table 6 lists the calculated torque value when a wire starts to yield. For example, the largest wire, d = 180 mm yields at 0.11 N-mm. Even the most sensitive torque cell did not have the required resolution for the largest size copper wire, and it was necessary to use the custom made torque sensor setup on Bionics.

During the period of this investigation, only one size of glass fiber was available. Based on the calibration results in Figure 29, the wire yield condition, and the range of glass fiber length (typically, 5 mm < L_{fiber} < 100 mm), the estimated angle of rotation of the glass fiber is shown in Table 6. The measurement would be too noisy to obtain a clean normalized torque-rotation curve when the maximum rotation was less than a couple of degrees. Increase fiber length

would make the rotation larger; however, it would encounter other experimental difficulties such as vibration and air disturbance if the fiber is too long. Successful torsion experiments were limited on two large wire sizes, 180 and 30 μm. The dimensions of the glass fiber and copper specimen used in the experiments and the weight applied at the bottom of the copper specimen are tabulated in Table 7.

Table 6 Predicated torque and glass fiber rotation at Q/a^3 = 150 MPa

Wire diameter	Torque Q, N-mm	Rotation, degree	
d =2a, μm	Q/a^3 = 150 MPa	L_{fiber} = 5 mm	L_{fiber} = 100 mm
180	0.109350	**41.42**	828.41
30	0.000506	0.19	**3.84**
20	0.000150	0.06	1.14
15	0.000063	0.02	0.48
12	0.000032	0.01	0.25

Table 7 Experiment parameters

Test	*d* mm	L_{fiber} mm	L_{Cu} mm	*mass* g
0070_7	179.7	25.4	6.4	2.0
0012_4	29.9	88.9	1.0	1.0

5.3.1 Result of w007 torsion experiment

The two parameters measured during the experiment were actuator rotation θ_T and sensor module rotation θ_S. The history of loading is plotted in Figure 31. From θ_S, the calculated shear strain rate at the surface of the copper specimen was about 2.3×10^{-6} s^{-1}. Based on the procedures described in section *5.1.2*, the torque was obtained and the normalized torque-rotation curve is shown in Figure 32. A line that fits the linear portion of the torque-rotation curve is also plotted in the figure. The curve deviates from the line at about 135 MPa, where the specimen started to yield.

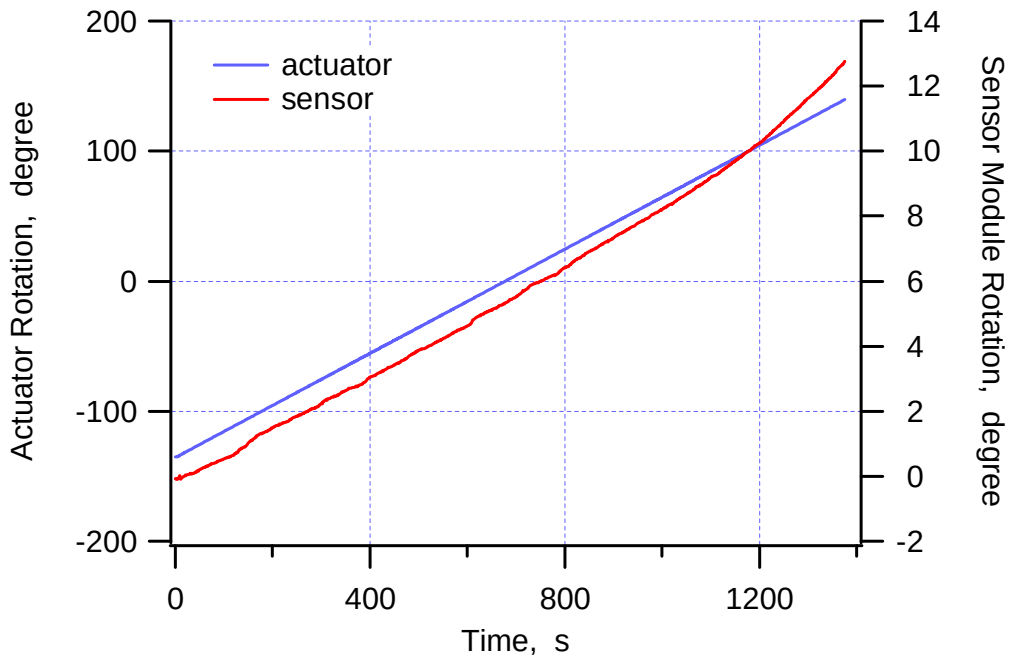

Figure 31 Measured actuator and sensor module rotations versus time of 007_7 test.

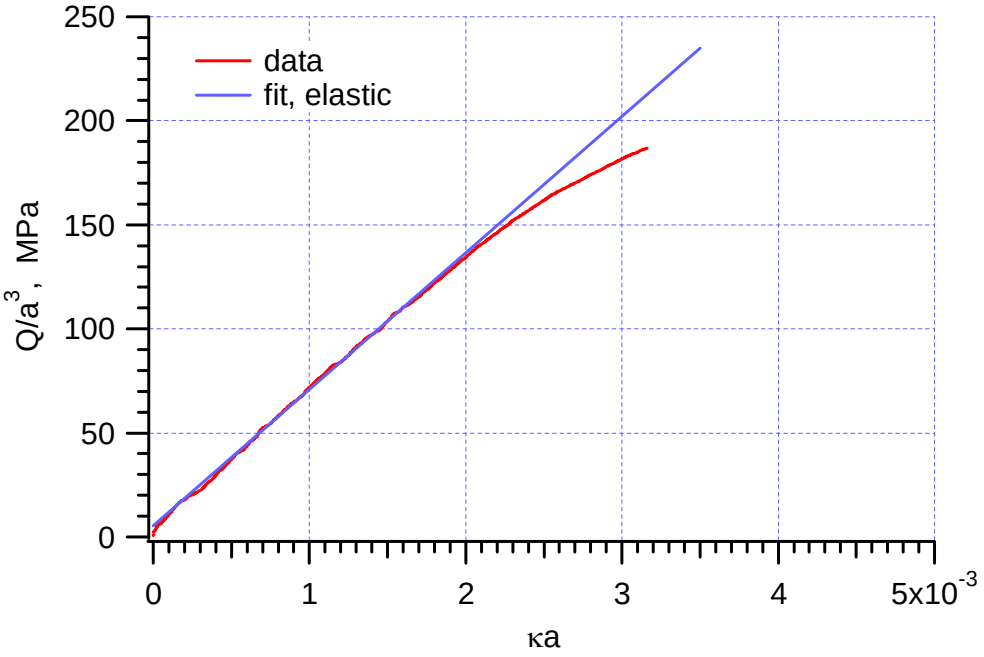

Figure 32 Normalized torque-rotation curve of w007 (Cu wire *d* = 180 μm).

5.3.2 Result of w0012 torsion experiment

In this experiment, the length of the glass fiber needed to be much longer than that in the previous test (see Table 7) so the plastic deformation would happen at a larger angle of twist (see Table 6). In addition, some improvements, shown in Figure 33, were also made on the sensor module to obtain a higher resolution of angle measurement: (1) the reference reflection tape was attached to the foam cylinder, instead of the actuator shaft, to minimize the effect of unwanted foam transverse motion (from vibration or air disturbance, etc.) during test; (2) the measuring reflection tape was bonded on the paper with a steeper angle, which amplified the angle-distance conversion.

The deformation history and the normalized torque-rotation curve are shown in Figure 34 and Figure 35, respectively. The shear strain rate was about 4.0×10^{-6} s^{-1}. The specimen yielded at a normalized torque of about 150 MPa, which is slightly higher than that of w007.

5.3.3 Summary

A delicate torsion setup was devised. The torque was measured through the rotation of a glass fiber. Using the glass fiber d =125 μm, the torque resolution is better than 1.0×10^{-4} N-mm, much better than commercially available torque cells. Even with that accuracy, it can obtain the stress-strain curve of only two largest sizes, w007 and w0012. To characterize the smallest w0005 copper wire, the glass fiber with diameter smaller than 50 μm should do the work.

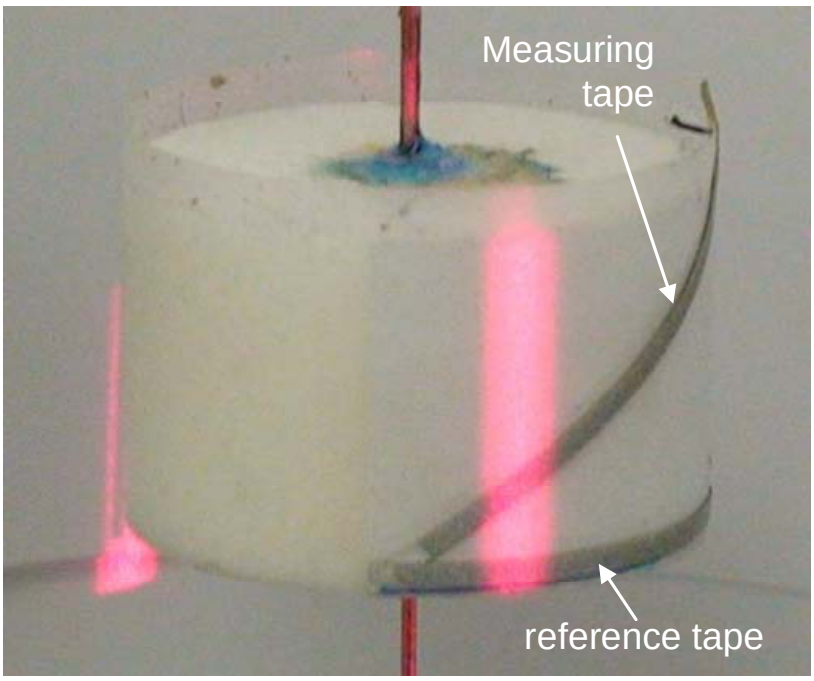

Figure 33 Improved sensor module

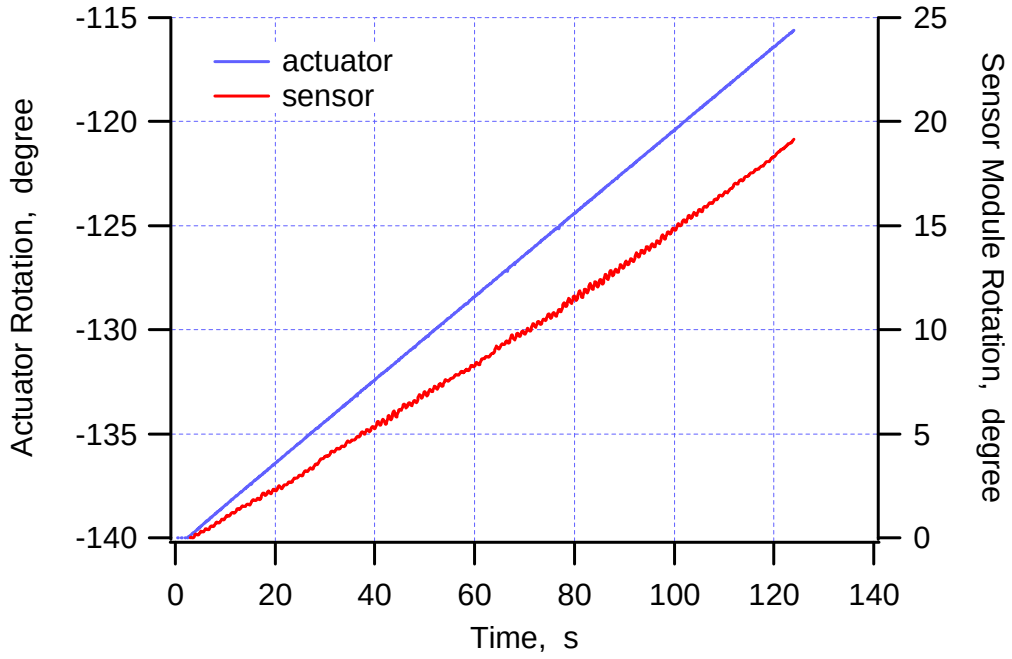

Figure 34 Measured actuator and sensor module rotations versus time of 0012_4 test.

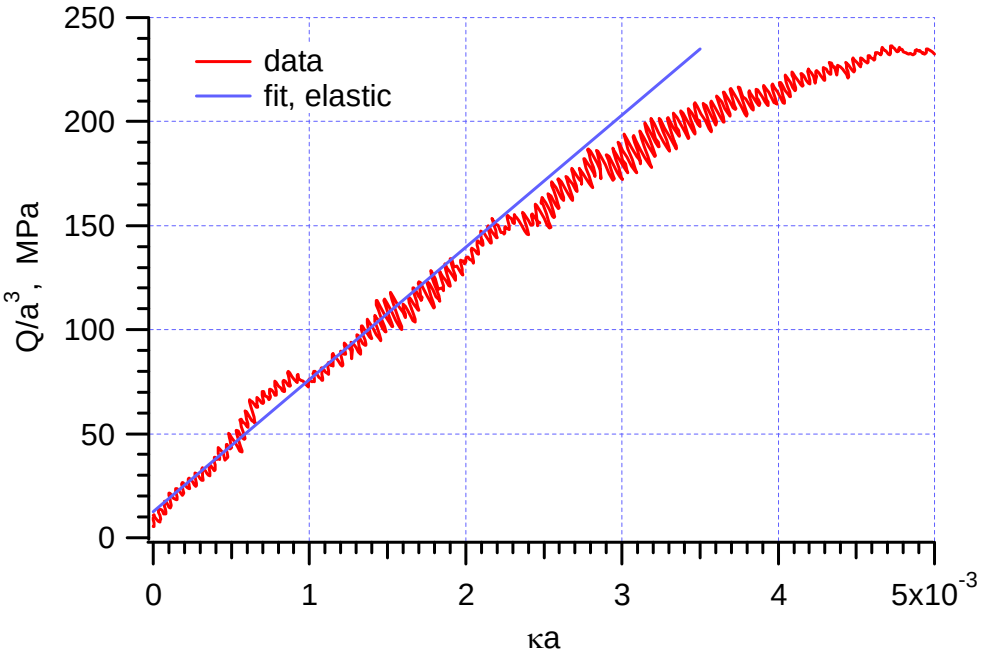

Figure 35 Normalized torque-rotation curve of w0012 (Cu wire *d* = 30 μm).

6. CONCLUSIONS

Analytical and experimental investigations were conducted to understand size effects intended for further developing predictive models. The focus was placed on the measurement of size effect by interrogating the most influential experiments by Fleck *et al*.

This simplified analytical study illustrates that variances in the tensile response are amplified in the torsion response. The amplification cannot explain the differences in torsion displayed in the experiment but the simplified analysis does yield a measure of that amplification.

Tension and torsion experiments of various thin copper wires were performed. EBSD technique was used to examine wire samples in the SEM. The microstructures of the wires used in the current experiments are very similar, containing many annealing twins but no significant texture present. Larger size wire has a larger average grain size. The average grain size of all wires is at the same order of magnitude. The variation in grain size within a wire, however, is quite large.

Tensile experiments were successfully conducted on all selected sizes with at least two repeats. The scattering of the plastic behaviors observed within the same size specimens may be explained by the pre-experiment deformation due to handling. The spread of yield stress and differences in hardening rate among various sizes demonstrate that there are some material variations and are not size related.

Normalized shear stress-strain curves were obtained for the largest two sizes w007 and w0012. The available glass fiber was not able to measure smaller size wires. The spread of normalized shear yield stress between w007 and w0012 was 15 MPa compared to a 50 MPa in the spread in the tensile yield stress.

A better understanding of size effect issues, innovative experimental and analytical methods, and size-effect measurement methodology have resulted from this brief investigation, which prepares us for further size effects research and development of predictive models.

7. REFERENCES

1. N. A. Fleck , G. M. Muller , M. F. Ashby And J. W. Hutchinson, Strain Gradient plasticity: Theory and Experiment, *Acta metall, mater.* Vol. 42, No. 2, pp. 475-487, 1994.

2. J. S. Stolken And A. G. Evans, A Microbend Test Method For Measuring The Plasticity Length Scale, *Acta Mater. Vol. 46, No. 14, Pp. 5109-5115, 1998.*

3. H.D. Espinosa, B.C.Prorok, B. Peng, Plasticity size e'ects in free-standing submicron polycrystalline FCC -lms subjected to pure tension, *Journal of the Mechanics and Physics of Solids,52, 667 – 689, 2004.*

4. J. R. Greer, W. C. Oliver, W. D. Nix, Strain Size dependence of mechanical properties of gold at the micron scale in the absence of strain gradients, *Acta Materialia 5, 1821–1830, 2005*.

5. Goodfellow Corporation, 305 High Tech Drive, Oakdale, PA 15071.

6. Six-Axis Force/Torque Transducer Installation and Operation Manual (NANO17), ATI Industrial Automation, Pinnacle Park, 1031 Goodworth Drive, Apex, NC 27539.

8. DISTRIBUTION

1	MS9042	Mike Chiesa	08776
1	MS9042	Davina Kwon	08770
5	MS9042	James W. Foulk III	08776
5	MS9042	Wei-Yang Lu	08776
1	MS9402	Nancy Yang	08772
1	MS9404	Bo Song	08776
1	MS9405	Bob Carling	08700
1	MS9409	Kevin Connelly	08776
2	MS9018	Central Technical Files	8944
2	MS0899	Technical Library	4536

For LDRD reports, add:

1	MS0123	D. Chavez, LDRD Office	1011

For Patent Caution reports, add:

1	MS0161	Patent and Licensing Office	11500


Sandia National Laboratories